Journal of Molecular Catalysis A: Chemical 331 (2010) 58–63

Contents lists available at ScienceDirect

Journal of Molecular Catalysis A: Chemical

journal homepage: www.elsevier.com/locate/molcata

Titania nano-photocatalysts synthesized by ultrasound and microwave methodologies: Application in depuration of water from 3-chloropyridine

Juan Carlos Colmenares[a,*], Maria A. Aramendia[b], Alberto Marinas[b], Jose M. Marinas[b], Francisco J. Urbano[b]

[a] Institute of Physical Chemistry, Polish Academy of Sciences, ul. Kasprzaka 44/52, 01-224 Warsaw, Poland
[b] Department of Organic Chemistry, University of Córdoba, Edificio Marie Curie, Ctra Nnal IV, Km 396, E-14014, Córdoba, Spain

ARTICLE INFO

Article history:
Received 8 June 2010
Received in revised form 22 July 2010
Accepted 29 July 2010
Available online 11 August 2010

Keywords:
Sol–gel method
Ultrasound
Microwave
Nanomaterials
Titania
Pyridine herbicides destruction
Water purification

ABSTRACT

The effect of aging the gel under ultrasonic (us) and microwave (mw) irradiation on the characteristics of the synthesized solids was studied. Sonication ensured the obtention of pure anatase nanoparticles in high crystalline state and generally led to obtain a high surface area and more active photocatalyst. Catalysts were characterized by a wide range of physical techniques (ICP-MS, N_2 isotherms, XRD, UV–vis and TEM). The total degradation of 3-chloropyridine was studied under titania-based photocatalysts, this degradation followed a zero-order kinetics respect to 3-chloropyridine. In our conditions, 100 ppm of 3-chloropyridine was degraded completely within ca. 8 h of UV-radiation (365 nm wavelength) on bare-titania systems. Some reactions intermediates were identified by SPME-GC–MS and a plausible mineralization route was suggested implying two parallel routes with hydroxylation and ring opening prior to or after the release of chloride ions. The modification of titania surface with metals (Fe, Pt, Pd) was detrimental for photocatalysis.

© 2010 Elsevier B.V. All rights reserved.

1. Introduction

One of the fields of the widest application of nanostructured materials has become the heterogeneous photocatalysis [1–4]. It is precisely the photocatalysis which is one of the significant areas of science which is gaining more and more force due to the multidisciplinary as well as multipurpose character of the solutions born from it. TiO_2 in the anatase form appears to be the most efficient material for environmental applications.

The most-widely used method to produce titania is the sol–gel method one. It seems that potentially photoactive titania particles should posses high surface area, high crystalline state and consist exclusively or predominantly in anatase nanoparticles. In this sense, the use of ultrasonic irradiation during the synthetic procedure has been reported to help to obtain smaller homogeneous nanoparticles and lead to an increase in surface area [5,6].

Unfortunately, titania photocatalyst has some drawbacks such as: (i) The relatively high electron–hole recombination rate, which is detrimental to its activity, (ii) the absorption in the UV-region, and (iii) the low surface area. In this sense, doping with metals could make a double effect: (i) firstly, it could reduce the band gap energy [7], thus shifting the absorption band to the visible region, and (ii) secondly, metals could provoke a decrease in electron–hole recombination rate, acting as electron traps [8].

The use of TiO_2 as photocatalyst for environmental cleanup has been of interest, because TiO_2 is stable, harmless, inexpensive, and solar activated [9–13].

Many pyridine derivatives have found widespread use as pesticides [14,15]. Efficiency of the pesticide is certainly its very important characteristic. Degradability, however, is a trait of equal, if not of greater importance. Namely, after plant treatment most pesticides end up in water flows, which are in most cases subsequently used for human or animal consumption. For this reason, a great deal of attention has been recently devoted to the degradation of pesticides as means of water decontamination.

The present piece of work is aimed at exploring the effect of microwave and ultrasound radiation during the materials synthesis (aging step of sol–gel method) on the structure and photocatalytic activity of these titania-based materials in the photocatalytic degradation of 3-chloropyridine (3-ClPy) in water. 3-ClPy was taken as model molecule of pyridine herbicides (picloram, aminopyralid or clopyralid). For comparative purpose, it has been prepared a reference TiO_2-material by a conventional reflux (r) method.

* Corresponding author. Fax: +48 22 6325276.
E-mail addresses: jcarlos@ichf.edu.pl, jcarlos@wp.pl (J.C. Colmenares).

1381-1169/$ – see front matter © 2010 Elsevier B.V. All rights reserved.
doi:10.1016/j.molcata.2010.07.014

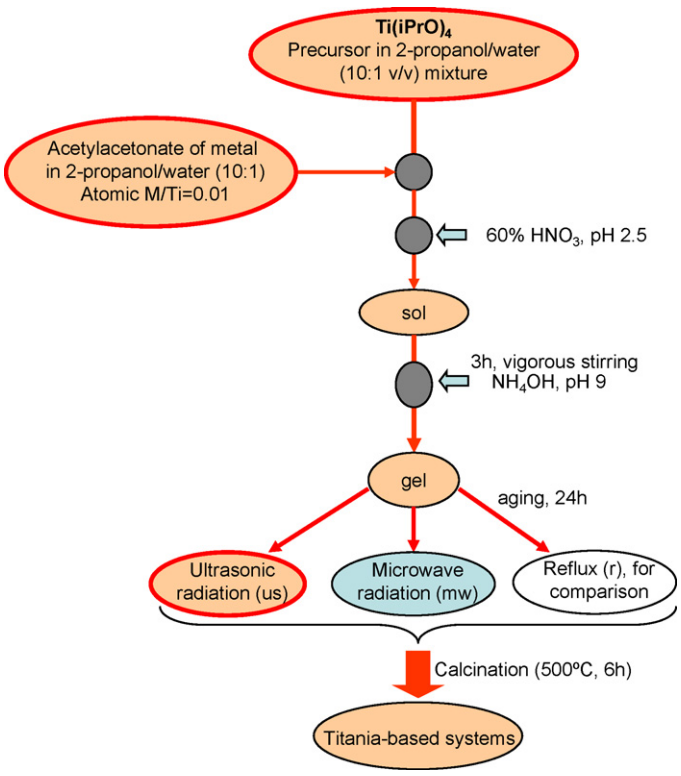

Fig. 1. Schematic representation of synthetic procedure to obtain pure- and metal-containing titania systems applied in the present work.

2. Experimental

2.1. Chemicals and catalysts preparation

Pure 3-ClPy (99%) was provided by Sigma–Aldrich. Sulphuric acid (98%), sodium nitrate, sodium nitrite, sodium chloride, anhydrous sodium acetate, sodium hydroxide, 37% hydrochloric acid and L-(+)-tartaric acid were purchased from Panreac. Sodium carbonate and bicarbonate, 2,6-pyridinedicarboxilic acid (dipicolinic acid) and sodium and ammonium formate were provided by Sigma–Aldrich. Finally, formic acid was provided by Merck. All reactives were used without any pre-treatment.

Photocatalytic mineralization tests were carried out using titanium dioxide alone as well as titania modified with different transition metals (Fe, Pd, Pt, in a metal/Ti nominal ratio equal to 0.01) prepared by sol–gel method. The catalysts synthesis was carried out (pH 9 with NH_4OH) using titanium tetraisopropoxide and the corresponding metal acetylacetonates as the titanium and metal precursors, respectively. The gels were aged under ultrasonic irradiation (Ultrasonic Homogenizer 4710 Series, Cole-Palmer Instrument Co. 300 W, 20 kHz, operated in the continuous mode) at 5 °C to avoid solvent evaporation, and microwave irradiation (CEM Focused Microwave™ Synthesis system, operating at a continuous microwave power of 140 W) for 24 h and calcined at 500 °C for 6 h in the air (see more details of the synthesis in Fig. 1). TiO_2(r) was also prepared by a reflux method (heated under vigorous stirring at propan-2-ol reflux temperature) and used as catalyst for comparison.

Water used for preparation of samples was Milli-Q quality water (Millipore Iberica, Spain).

2.2. Standard solutions

3-ClPy calibration was carried out from solutions of pure 3-ClPy in water in the range of 10–200 mg/L ($r^2 \approx 1$), analysed by HPLC-DAD.

Concerning anion calibration, standard solution containing $NaNO_3$ (nitrate determination), $NaNO_2$ (nitrite), NaCl (chloride), $CH_3CO_2NH_4$ (acetate) and CHO_2NH_4 (formiate) in the range of 2–30 mg/L were prepared. Regarding ammonium detection, $HCOONH_4$ solutions (2–16 mg/L) were used. For all cases, correlation coefficients obtained for calibration curves were over 0.99.

2.3. Photocatalytic tests

All catalytic tests were performed in a Pyrex cylindrical double-walled immersion well reactor (23 cm long × 5 cm internal diameter, with a total volume of ca. 450 cm^3) open to air. Irradiation of the reaction solutions was carried out by using a medium pressure 125 W Hg lamp (λ_{max} = 365 nm) supplied by Photochemical Reactors Ltd. (Model 3010). Water used for cooling was thermostated at 20 °C. Lamp output was calculated to be ca. 1.5×10^{-3} Einstein/s (ferrioxalate actinometry method). Constant agitation (1100 rpm) of the suspension was insured by a magnetic stirrer placed at the reactor base.

Solutions of pure 3-ClPy were prepared in Milli-Q water and kept in the dark at 4 °C. Such solutions were never used for more than 4 days. Experiments were carried out from 200 mL of the mother solution (25–100 ppm of 3-ClPy) and 1.5 g L^{-1} of catalyst concentra-

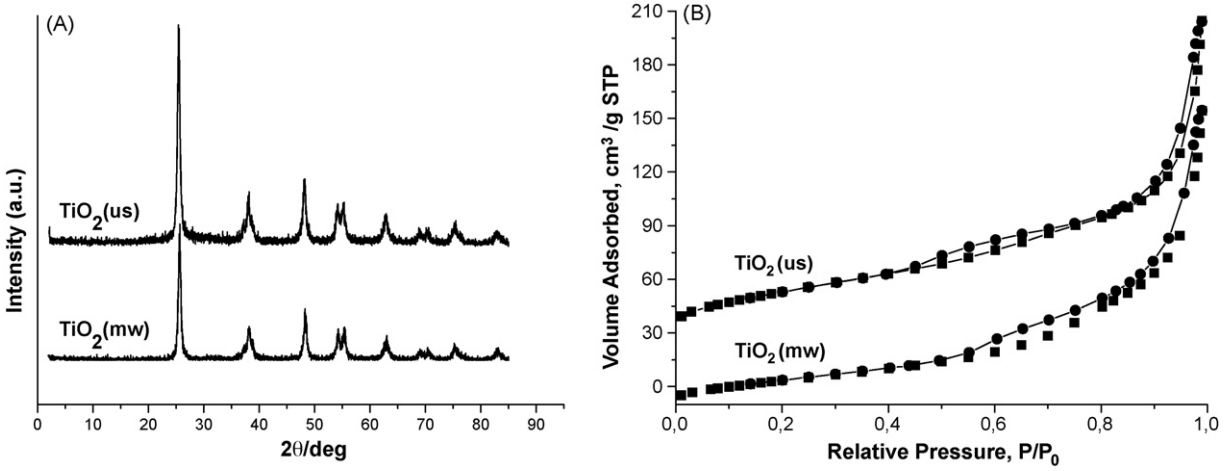

Fig. 2. (A) X-ray diffraction patterns corresponding to the TiO_2(us) and TiO_2(mw) systems, (B) N_2 adsorption (square symbols)–desorption (circle symbols) isotherms obtained at liquid nitrogen temperature for the TiO_2(us) and TiO_2(mw) systems.

Table 1
Main features of the characterization concerning the different titania-based systems applied in the present research work.

Catalyst	N_2 isotherms[a]			ICP-MS		XRD		UV–vis	
	S_{BET} ($m^2\ g^{-1}$)	V_p (mL/g)	d_p (Å)	Nominal content (metal/Ti %)	Experimental (metal/Ti %)	Anatase crystal phase (%)	Crystalline size of phase (nm)	Band gap (eV)	Absorption threshold (nm)
TiO_2(r)	60	0.23	140	–	–	100	21	3.19	389
TiO_2(mw)	71	0.28	129	–	–	100	17	3.19	389
TiO_2(us)	121	0.29	93	–	–	100	19	3.19	389
Fe–TiO_2(us)	61	0.22	126	1.0	1.7	100	20	3.15	394
Pd–TiO_2(us)	75	0.23	106	1.0	0.6	100	20	3.12	397
Pt–TiO_2(us)	57	0.23	143	1.0	0.5	100	23	3.13	396

[a] Specific surface area (S_{BET}), cumulative pore volume (V_p) and pore mean diameter (d_p).

tion was used. The mixture was maintained in the dark for 20 min under stirring (1100 rpm) to reach adsorption equilibrium, and was then irradiated. All degradation experiments were carried out at room temperature and unless otherwise stated bubbling through the suspension an O_2/N_2 (10:90, v/v) mixture at 80 mL min^{-1}.

The production of ions and carbon dioxide was carried out for the best catalysts in the photodegradation of 3-ClPy.

Experiments were performed three times and the results correspond to the average of the repetitions.

2.4. Analyses

2.4.1. Kinetic studies

Samples taken at different times of illumination were filtered through 0.22 μm, 25 mm Φ nylon filters provided by Tracers, in order to remove catalysts particles before analyses by HPLC-DAD. A Waters 2695 liquid chromatograph equipped with a quaternary solvent delivery system, an autosampler and a Waters 2996 DAD detector (λ = 210 and 266 nm for 3-ClPy) was used. HPLC apparatus was a Spectra-System P2000 Liquid Chromatograph (Spectra Physics) equipped with an automatic injector (Spectra-System AS3000), a Spectra-100 UV–vis detector and a Tracer Kromasil 100 C18 column (150 mm × 2.1 mm i.d., 5 μm particle diameter). The composition of the binary mobile phase (flow rate 0.2 mL min^{-1}) was 60% acetonitrile and 40% water (0.05% formic acid). The temperature of the analytical column was 30 °C and the injection volume 20 μL.

2.4.2. Mineralization studies

Evolution of inorganic ions (NO_3^-, NO_2^-, Cl^-, CH_3COO^-, $HCOO^-$, NH_4^+) was followed by conductivity HPLC. Quantification was possible using the corresponding calibration curve. The HPLC system used comprised a Metrohm Metrosep anion dual two column (75 mm × 4.6 mm i.d., 5 μm particle diameter), a Metrohm 753 ionic suppression module (using sulphuric acid for regeneration of cartridges) and Metrohm 732 ionic conductivity detector. Mobile phase was mixture of Na_2CO_3 (1.3 mmol L^{-1}) and $NaHCO_3$ (2.0 mmol L^{-1}), flow rate was 0.8 mL min^{-1}. Injection volume was 10 μL.

For ammonium ion determination, ion suppression module was not necessary and a Metrohm Metrosep C2 100 column (100 mm × 4.0 mm i.d., 5 μm particle diameter) was used. Mobile phase was a mixture of dipicolinic acid (0.75 mmol L^{-1}) and L-(+)-tartaric acid (4 mmol L^{-1}), flow rate was 1 mL min^{-1}. Injection volume was 10 μL.

2.4.3. Intermediate products evaluation

Reaction products were followed by SPME-GC–MS using a CP-3800 Gas Chromatograph connected to a Varian 1200 Quadrupole MS. A Supelcowax-10 capillary column (0.25 μm film, 60 m × 0.25 mm) was used.

Different fibers were tested as absorbents (polyacrylate, PDMS/DVB, etc). The best one had polyacrylate as the stationary phase (Supelco 57305). Before using, the fiber was conditioned at 300 °C for 2 h. It was then introduced in the vial containing the filtered sample which was extracted at 40 °C and 500 rpm for 30 min. Masses were scanned in the 30–300 amu range. Moreover, selective extraction of ions helped us to detect the presence of low contents of certain intermediates in the total ion chromatogram. Main selected peaks were *m*/*z* 79 (pyridine), 113 and 115 (3-chloropyridine), 95 and 111 (hydroxylated pyridines), 129, 131, 145, 147, 161 and 163 (hydroxylated chloropyridines). Nev-

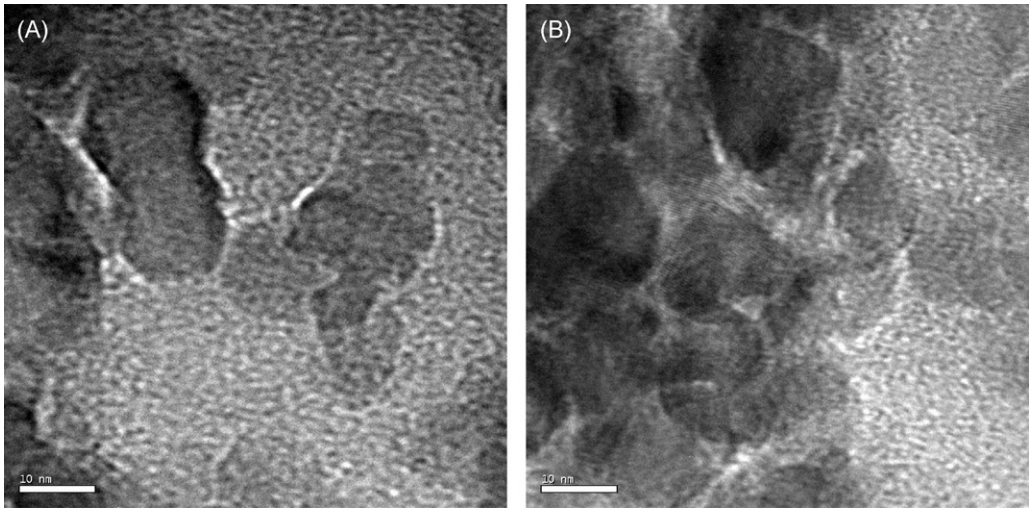

Fig. 3. TEM micrographs of TiO_2(mw) (A) and TiO_2(us) (B).

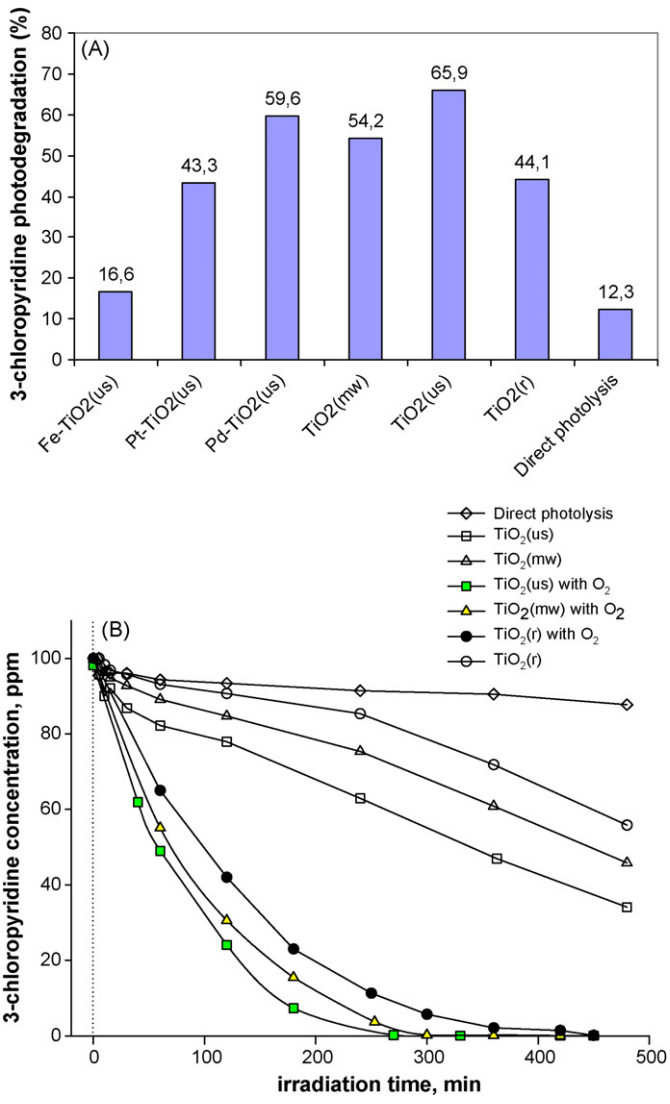

Fig. 4. Photodegradation of an aqueous solution (200 mL) containing 100 ppm of 3-chloropyridine and 1.5 g L^{-1} of catalyst. (A) Grade of photodegradation obtained with different titania-based systems after 8 h of UV irradiation in a reactor open to the air. (B) Comparative studies using TiO_2(us), TiO_2(mw) and TiO_2(r) systems with and without O_2 bubbling as well as for direct photolysis.

ertheless, all the products were characterized by comparing the molecular ion and fragmentation pattern with those reported in the GC–MS library.

2.5. Characterization of titania-based photocatalysts

The textural properties of solids were determined from nitrogen adsorption–desorption isotherms at liquid nitrogen temperature by using a Micromeritics ASAP-2010 instrument. Specific surface areas were calculated by the BET method, while pore distributions were determined by the BJH method. Prior to measurements, all samples were degassed at 110 °C to 0.1 Pa for 3 h.

Elemental analysis of catalysts was carried out on a ICP-MS ELAN-DRC-e (Perkin-Elmer), after dissolution of the sample in a H_2SO_4:HF:H_2O (1:1:1) mixture. Atomic spectroscopy standard PE Pure Plus no. 4 (Perkin-Elmer) was used for calibration.

X-ray analysis of solids was carried out using a Siemens D-5000 diffractometer provided with an automatic control and data acquisition system (DACO-MP). The patterns were run with nickel-filtered copper radiation (λ = 1.5406 Å) at 40 kV and 30 mA; the

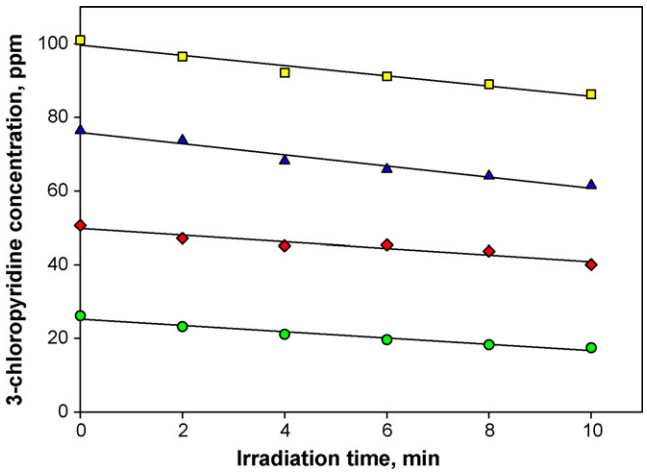

Fig. 5. Kinetic studies on TiO_2(us) evidencing the zero-order with respect to 3-chloropyridine.

diffraction angle 2θ was scanned at a rate of 2° min^{-1}. The average crystallite size of anatase was determined according to the Scherrer equation using the full-width at half-maximum (FWHM) of the peak corresponding to 1 0 1 reflection, and taking into account the instrument broadening.

Diffuse reflectance UV–vis spectra were performed on a Cary 1E (Varian) instrument, using barium sulphate as reference material. Band gap values were obtained from the plot of the Kubelka–Munk function $[F(R_\infty)E]^{1/2}$ versus the energy of the absorbed light E. Extrapolation to $y = 0$ of the linear regression in the 3.4–3.7 eV range afforded the band gap energy E_{gap} (eV) [16,17]. Regarding absorption threshold, it was determined according to the formula [18]:

$$\lambda = \frac{hc}{E_{gap}} = \frac{1240}{E_{gap}}$$

Transmission electron microscopy (TEM) images were recorded in a JEOL JEM 2010 microscope operating at an accelerating voltage of 200 kV. The structural resolution of this microscope is 0.19 nm. Samples were previously embedded in an epoxy resin. Sections with a thickness of 40 nm were finally obtained with an ultramicrotome and mounted on 3-mm holey carbon copper grids.

3. Results and discussion

3.1. Photocatalysts characterization

The main features concerning characterization of all systems are summarized in Table 1 and Figs. 2 and 3.

Textural properties of the catalysts are summarized in Table 1 and Fig. 2B. In general, sonication treatment resulted in a significant increase in surface area. Such results show the important effect of sonication on the textural properties not only during the sol or gel formation [19,20] but also during the subsequent gel evolution as it is reported in our work. This is particular remarkable in the case of TiO_2(us), for which the highest surface area (121 m^2 g^{-1}) together with a great decrease in pore size were observed.

After calcinations, metal content of the solids was determined by ICP-MS. Results are shown in Table 1. The discrepancies between the nominal and experimental metal/Ti ratios can be explained in terms of the solubility of the different metal species at pH used for precipitation (pH 9).

The X-ray diffraction patterns of the catalysts allowed us to identify the crystal phases present in the catalysts (Table 1 and Fig. 2A). Aging either under sonication or under microwave irradi-

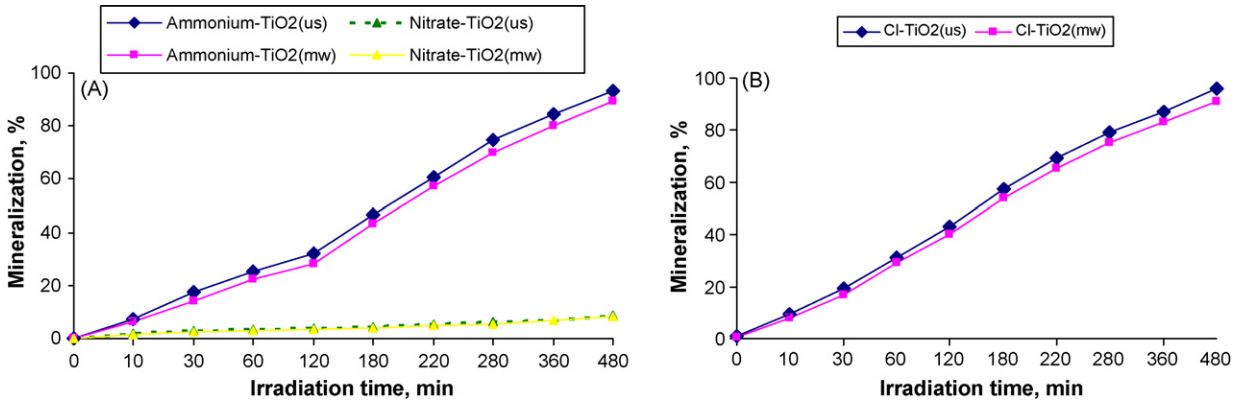

Fig. 6. Heteroatoms monitoring on TiO_2(us) and TiO_2(mw). (A) Nitrogen evolution (ammonium/nitrate). (B) Chloride ions evolution.

ation ensured the obtention of pure anatase and generally resulted in smaller particles. As it can be seen in Fig. 2A the grade of crystalline state for TiO_2(us) is higher than for TiO_2(mw) and much higher than TiO_2(r) (image not shown), this feature is very important in photocatalysis due to the reduction of recombination rate of electron–hole pair which is of paramount importance in obtaining more stable and active photocatalysts. As shown in our work, only aging the gel under ultrasonic irradiation lead to obtain a pure anatase nanoparticles in high crystalline state with the highest surface area among all materials prepared in this research work.

In order to obtain some information on the potential application in photocatalysis of our solids UV–vis spectra were obtained. UV–vis data collected in Table 1 seem to indicate that in our solids no quantum size effect is observed, as shown by the fact that TiO_2(us) and TiO_2(mw) with anatase crystallite size as different as 19 and 17 nm, respectively, exhibit identical gap energy values. Furthermore, the presence of Fe, Pd and Pt leads to a shift of absorption band to the visible region (red shift).

TEM micrographs of TiO_2(mw) and TiO_2(us) are represented in Fig. 3. TEM images confirm that aging under sonication normally leads to smaller particles. Moreover, particles resulting from ultrasonic radiation are more spherical than the polyhedrical-shaped ones obtained by microwave radiation; the same particles shape was observed for TiO_2(r) (images not shown).

3.2. Kinetics of 3-chloropyridine disappearance

The fact that the reaction volume was 200 mL allowed us to sample 10 times at each experience (2 mL each), thus avoiding significant mistakes due to the sampling of an excessive volume (volume variation ca. 10%).

The use of a diode array detector allowed us to check peak purity trough simultaneous quantification at several wavelengths. For 3-chloropyridine, determination was performed at 210 and 266 nm which correspond to two absorption maxima in UV absorption spectrum of 3-chloropyridine. Fig. 4A shows the results found after 8 h UV irradiation for photocatalytic degradation of 3-chloropyridine (100 ppm in water) in a reactor open to the air (no O_2 bubbling). As shown in this figure, the best results in terms of 3-ClPy degradation are obtained with TiO_2(us) and TiO_2(mw). Modifying the bare-titania with Fe, Pd or Pt does not increase the photocatalytic activity in this reaction, even though, such doping is particularly detrimental for iron metal. Comparing (Fig. 4A and B) the photodegradation of 3-ClPy with and without O_2 between pure titania synthesized by aging the gel under ultrasonic irradiation and aging the gel under microwave irradiation, it can be seen that the high surface area of TiO_2(us) (121 $m^2\,g^{-1}$) and high crystalline state is influencing positively on a faster photodegradation of 3-ClPy than in the case of TiO_2(mw) (S_{BET} = 71 $m^2\,g^{-1}$) (Fig. 4B). The worse results in the matter of 3-ClPy degradation were obtained for our reference TiO_2(r) (S_{BET} = 60 $m^2\,g^{-1}$). Moreover, it seems that the high grade of crystalline state of TiO_2(us) (Fig. 2A) can help to reduce the rate of recombination of electron–hole pair during the photocatalytic process ensuring to obtain a highly stable and photoactive solid.

Results achieved for this screening prompted us to select the most active photocatalytic systems TiO_2(us), TiO_2(mw) and a reference TiO_2(r) for further studies on 3-ClPy photocatalytic degradation.

Fig. 4B shows a typical degradation kinetic curve for 3-ClPy (100 ppm in water) on TiO_2(us), TiO_2(mw) and TiO_2(r) at 210 nm. Empty symbols are related to the experiments carried out with the reactor open to the air whereas results obtained for reactions in which an O_2/N_2 (10:90, v/v) flow was bubbled through the suspension are represented with full symbols. The curves found at 266 nm were exactly the same, thus overlapping with those at 210 nm. As can be seen, there is no practically reaction in the absence of photocatalyst. Moreover, reaction is much more faster when oxygen is bubbled into the suspension. Lastly, 3-ClPy degradation is definitively better with TiO_2(us) than with TiO_2(mw) and TiO_2(r) which prompted us to select the former catalyst, with O_2 bubbling, for more accurate kinetic studies.

Results obtained from the reactions performed at different 3-ClPy initial concentrations in order to determine the substrate partial order are presented in Fig. 5. As shown in this figure, degradation follows a zero kinetic order with a rate being constant, regardless of the initial concentration, and equal to 1.5×10^{-5} mol L^{-1} min^{-1}. This kind of kinetics is in agreement with the results reported elsewhere for 3-amino-2-chloropyridine [21].

3.3. Mineralization monitoring

The mineralization of an organic compound by photocatalysis, generally give us gaseous CO_2 and inorganic anions coming from heteroatoms which remain in solution. In the case of 3-ClPy, one can expect the formation of NO_2^-, NO_3^- and/or NH_4^+ as well as Cl^-. The overall equation, valid after long irradiation time in oxygen excess, which describes photocatalytic mineralization of 3-ClPy is shown below:

$$C_5H_4NCl + 7O_2 \rightarrow \text{Intermediates} \rightarrow 5CO_2 + HNO_3 + HCl + H_2O$$

Heteroatoms evolution is presented in Fig. 6. In accordance with that observed for 3-ClPy disappearance, mineralization process is faster for TiO_2(us) and for both tested systems (specially for TiO_2(us) than for TiO_2(mw)) mineralization is practically completed (>95%) after 480 min of irradiation. As far as nitrogen is

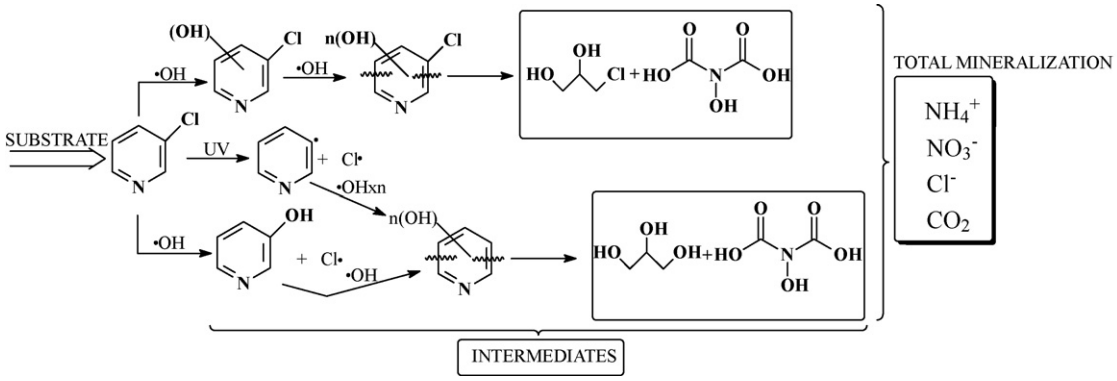

Fig. 7. Plausible degradation pathway suggested for 3-chloropyridine photocatalytic degradation.

concerned, the main product is ammonium, nitrate is only present as minor product (5–9%) and nitrite is not observed (Fig. 6A), this is in agreement with other studies on photocatalytic degradation of chemicals containing a pyridine ring [12,21].

Therefore, mineralization was complete for 3-ClPy which is of paramount importance since, otherwise, it could have been transformed into even more contaminant species.

The fact that inorganic anions evolution (specially for nitrate and chloride anions) showed a complete mineralization after at ca. 480 min of irradiation prompted us to take samples at time intervals below such a value (ca. after 200 min of irradiation) in order to monitor evolution of reaction intermediates. To monitor the evolution of intermediates different samples were analyzed by GC–MS (direct injection) and SPME-GC–MS. In view of the results, a plausible degradation pathway for 3-chloropyridine degradation is proposed (Fig. 7). Therefore, the existence of two parallel routes is suggested. Such routes involve hydroxylation and ring opening prior to (up-hand route) or after (down-hand one) the release of chloride ions.

Hydroxylation of the ring prior to the chloride release would explain that 3-chloropyridine disappears at higher rate than chloride species are formed. Furthermore, unidentified peaks in HPLC-DAD chromatograms of 3-chloropyridine photodegradation, could correspond to hydroxylated chloropyridines, whose absorption spectra will probably be quite similar to that of 3-chloropyridine. Finally, acetic and formic acids were also detected by anionic HPLC.

4. Conclusions

The synthesis of titania by ageing the gel under ultrasonic irradiation gave us a better solid material (100% anatase nanoparticles, high crystalline state and high surface area) than other materials synthesized either by microwave or reflux methodology. The best photocatalytic performances in the degradation of 3-ClPy was obtained when TiO_2(us) was used. Doping of titania with metals was detrimental for photocatalysis. Under our experimental conditions, total mineralization (absence of highly toxic compounds in water) of 100 ppm of 3-ClPy aqueous solution was achieved within 8 h of irradiation. Kinetic studies showed a zero-order with respect to 3-ClPy. Degradation pathway studies carried out by SPME-GC–MS allowed us to propose a tentative mineralization route consisting of two parallel ways involving hydroxylation of the aromatic ring prior to or after chlorine release.

Acknowledgments

The authors wish to acknowledge the staff at the Central Service for the support of research (SCAI) at the University of Cordoba for ICP-MS and TEM measurements.

This research was supported by a Marie Curie International Reintegration Grant within the 7th European Community Framework Programme. The authors thank for the support from the Consejeria de Educacion y Ciencia of the Junta de Andalucia and the Spanish Ministerio de Educacion y Ciencia.

References

[1] N. Serpone, A.V. Emeline, Res. Chem. Intermed. 31 (2005) 391–432.
[2] J.C. Colmenares, M.A. Aramendía, A. Marinas, J.M. Marinas, F.J. Urbano, Appl. Catal. A 306 (2006) 120–127.
[3] C.-G. Wu, C.-C. Chao, F.-T. Kuo, Catal. Today 97 (2004) 103–112.
[4] J.C. Colmenares, R. Luque, J.M. Campelo, F. Colmenares, Z. Karpiński, A.A. Romero, Materials 2 (2009) 2228–2258.
[5] J.C. Yu, J. Yu, W. Ho, L. Zhang, Chem. Commun. (2001) 1942–1943.
[6] C.W. Oh, G.D.L. Seong, S. Park, C.S. Ju, S.S. Hong, React. Kinet. Catal. Lett. 85 (2005) 261–268.
[7] X. Zhang, F. Zhang, K.-Y. Chan, Mater. Chem. Phys. 97 (2006) 384–389.
[8] P. Pichat, New J. Chem. 11 (1987) 135–140.
[9] C. Guillard, J. Disdier, C. Monnet, J. Dussaud, S. Malato, J. Blanco, M.I. Maldonado, J.M. Herrmann, Appl. Catal. B 46 (2003) 319–332.
[10] S. Malato, J. Blanco, A. Campos, J. Caceres, C. Guillard, J.M. Herrmann, A.R. Fernandez-Alba, Appl. Catal. B 42 (2003) 349–357.
[11] P. Pichat, in: M.A. Tarr (Ed.), Chemical Degradation Methods for Wastes and Pollutants: Environmental and Industrial Applications, Marcel Dekker Inc., New York, Basel, 2003, pp. 77–119.
[12] M.A. Aramendia, A. Marinas, J.M. Marinas, J.M. Moreno, F.J. Urbano, Catal. Today 101 (2005) 187–193.
[13] M.A. Aramendia, J.C. Colmenares, S. Lopez-Fernandez, A. Marinas, J.M. Marinas, J.M. Moreno, F.J. Urbano, Catal. Today 138 (2008) 110–116.
[14] R.J. Gilliom, J.E. Barbash, D.W. Kolpin, S.J. Larson, Environ. Sci. Technol. 33 (1999) 164A–169A.
[15] D.W. Kolpin, J.E. Barbash, R.J. Gilliom, Environ. Sci. Technol. 32 (1998) 558–566.
[16] S. Sakthivel, H. Kisch, Angew. Chem. Int. Ed. 42 (2003) 4908–4911.
[17] J.E. Herrera, D.E. Resasco, J. Phys. Chem. B 107 (2003) 3738–3746.
[18] Y. Miyake, H. Tada, J. Chem. Eng. Jpn. 37 (2004) 630–635.
[19] Y.Q. Wang, S.G. Chen, X.H. Tang, O. Palchik, A. Zaban, Y. Koltypin, A. Gedanken, J. Mater. Chem. 11 (2001) 521–526.
[20] J. Yu, M. Zhou, B. Cheng, H. Yu, X. Zhao, J. Mol. Catal. A 227 (2005) 75–80.
[21] B.F. Abramovic, V.B. Anderluh, A.S. Topalov, F.F. Gaal, Appl. Catal, Appl. Catal. B 48 (2004) 213–221.